



3 1176 00159 4085

Copy 44  
RM SL53104

UNCLASSIFIED

NACA

# RESEARCH MEMORANDUM

for the

U. S. Air Force

INVESTIGATION OF THE LOW-SPEED STABILITY AND CONTROL  
CHARACTERISTICS OF A 1/10-SCALE MODEL OF THE  
CONVAIR YF-102 AIRPLANE IN THE LANGLEY  
FREE-FLIGHT TUNNEL

By Joseph L. Johnson, Jr., and Peter C. Boisseau

Langley Aeronautical Laboratory  
Langley Field, Va.

CLASSIFIED DOCUMENT

This material contains information affecting the National Defense of the United States within the meaning of the espionage laws, Title 18, U.S.C., Secs. 793 and 794, the transmission or revelation of which in any manner to an unauthorized person is prohibited by law.

NATIONAL ADVISORY COMMITTEE  
FOR AERONAUTICS

WASHINGTON

UNCLASSIFIED

CLASSIFICATION CHANGED

UNCLASSIFIED

CLASSIFICATION CHANGED

to UNCLASSIFIED

2/3/58

UNCLASSIFIED

UNCLASSIFIED

## NATIONAL ADVISORY COMMITTEE FOR AERONAUTICS

## RESEARCH MEMORANDUM

~~Unavailable~~

for the

U. S. Air Force

## INVESTIGATION OF THE LOW-SPEED STABILITY AND CONTROL

## CHARACTERISTICS OF A 1/10-SCALE MODEL OF THE

## CONVAIR YF-102 AIRPLANE IN THE LANGLEY

## FREE-FLIGHT TUNNEL

By Joseph L. Johnson, Jr., and Peter C. Boisseau

## SUMMARY

An investigation of the low-speed, power-off stability and control characteristics of a 1/10-scale model of the Convair YF-102 airplane has been made in the Langley free-flight tunnel. The model was flown over a lift-coefficient range from 0.5 to the stall in its basic configuration and with several modifications involving leading-edge slats and increases in vertical-tail size. Only relatively low-altitude conditions were simulated and no attempt was made to determine the effect of freeing the controls.

The longitudinal stability characteristics of the model were considered satisfactory for all conditions investigated. The lateral stability characteristics were considered satisfactory for the basic configuration over the speed range investigated except near the stall, where large values of static directional instability caused the model to be directionally divergent. The addition of leading-edge slats or an 80-percent increase in vertical-tail area increased the angle of attack at which the model became directionally divergent. The use of leading-edge slats in combination with a 40-percent increase in vertical-tail size eliminated the directional divergence and produced satisfactory stability characteristics through the stall. The longitudinal and lateral control characteristics were generally satisfactory. Although the adverse sideslip characteristics for the model were considered satisfactory over the angle-of-attack range, analysis indicates that the adverse sideslip characteristics of the airplane may be objectionable at high angles of attack.

UNCLASSIFIED

## INTRODUCTION

An investigation of the low-speed stability and control characteristics of a 1/10-scale model of the Convair YF-102 airplane has been made in the Langley free-flight tunnel at the request of the U. S. Air Force. The YF-102 airplane is a turbojet-powered, interceptor-type airplane with a 60° delta wing and a 60° delta vertical tail.

The investigation included flight tests of the model in its basic configuration and with several modifications involving leading-edge slats and increases in vertical-tail size. Force tests were also made of these configurations to determine the static stability characteristics.

In order to permit a better interpretation of the free-flight-tunnel tests in terms of the full-scale airplane, a comparison was made between the results of force tests at low Reynolds numbers in the free-flight tunnel and force tests at higher Reynolds numbers made by Convair.

## SYMBOLS

All stability parameters and coefficients are referred to the stability system of axes originating at a center-of-gravity position of 30.0 percent of the mean aerodynamic chord and vertically on the longitudinal body axis of the model unless otherwise noted (see figs. 1 and 2).

S	wing area, sq ft
$\bar{c}$	mean aerodynamic chord, ft
V	airspeed, ft/sec
b	wing span, ft
q	dynamic pressure, lb/sq ft
$\rho$	air density, slugs/cu ft
W	weight, lb.
m	airplane mass, slugs
$\mu_b$	relative-density factor, $m/\rho S b$
$\beta$	angle of sideslip, deg ( $\beta = -\psi$ in force tests)

000

 $\psi$  angle of yaw, deg

0000

 $\phi$  angle of bank, deg

1000

 $\alpha$  angle of attack, deg $\eta$  inclination of principal longitudinal axis of airplane with respect to flight path, positive when principal axis is above flight path at the nose, deg $I_X$  moment of inertia about longitudinal body axis,  $mk_X^2$ , slug-ft<sup>2</sup> $I_Y$  moment of inertia about lateral body axis,  $mk_Y^2$ , slug-ft<sup>2</sup> $I_Z$  moment of inertia about normal body axis,  $mk_Z^2$ , slug-ft<sup>2</sup> $k_X$  radius of gyration about longitudinal body axis, ft $k_Y$  radius of gyration about lateral body axis, ft $k_Z$  radius of gyration about normal body axis, ft $X$  longitudinal force, lb $Y$  lateral force, lb $Z$  normal force, lb $M$  pitching moment, lb-ft $N$  yawing moment, lb-ft $L$  rolling moment, lb-ft $C_L$  lift coefficient, Lift/qS $C_D$  drag coefficient, Drag/qS $C_m$  pitching-moment coefficient,  $M/qS\bar{c}$  $C_n$  yawing-moment coefficient,  $N/qSb$  $C_l$  rolling-moment coefficient,  $L/qSb$

$C_Y$  lateral-force coefficient,  $Y/qS$

$$C_{Y\beta} = \frac{\partial C_Y}{\partial \beta} \text{ per deg}$$

$$C_{n\beta} = \frac{\partial C_n}{\partial \beta} \text{ per deg}$$

$$C_{l\beta} = \frac{\partial C_l}{\partial \beta} \text{ per deg}$$

$$C_{Yp} = \frac{\partial C_Y}{\partial \frac{pb}{2V}} \text{ per radian}$$

$$C_{lp} = \frac{\partial C_l}{\partial \frac{pb}{2V}} \text{ per radian}$$

$$C_{np} = \frac{\partial C_n}{\partial \frac{pb}{2V}} \text{ per radian}$$

$\delta_r$  rudder deflection in a plane perpendicular to hinge line, deg

$\delta_e$  elevator deflection perpendicular to hinge line (elevons deflected together for elevator control), deg

$\delta_a$  aileron deflection perpendicular to hinge line (elevons deflected differentially for aileron control), deg

$p$  rolling angular velocity, radians/sec

#### APPARATUS AND MODEL

The flight tests and static force tests were conducted in the Langley free-flight tunnel, which is designed to test free-flying dynamic models. A complete description of the tunnel and its operation is presented in reference 1. The rolling derivatives were measured on the rotary balance in the Langley 20-foot free-spinning tunnel which is described in reference 2.

The 1/10-scale model used in the investigation was constructed at the Langley Laboratory. A three-view drawing of the model is shown in figure 2 and a photograph of the model is shown in figure 3. Table I gives the mass and dimensional characteristics of the full-scale design and the scaled-up mass and dimensional characteristics of the model. Midspan leading-edge slats and three different-size vertical tails were also tested on the model (see fig. 2). The vertical tails tested were the basic tail (tail A), a tail with 40-percent increase in area (tail B), and a tail with 80-percent increase in area (tail C).

## DETERMINATION OF THE STATIC STABILITY AND CONTROL CHARACTERISTICS

## AND ROTARY DERIVATIVES OF THE FLIGHT TEST MODEL

## Force Tests to Determine Longitudinal Stability and Control

Force tests were made to determine the static longitudinal stability and control characteristics of the model over an angle-of-attack range from  $0^\circ$  through the stall for the model in its basic and modified configurations. All the force tests were run at a dynamic pressure of 2.7 pounds per square foot which corresponds to an airspeed of about 47.3 feet per second at standard sea-level conditions and to a test Reynolds number of 700,000 based on the mean aerodynamic chord of 2.32 feet.

Presented for comparison with the free-flight-tunnel data are higher Reynolds number data (Reynolds number, 3,400,000) obtained from tests conducted at Convair (ref. 3). The longitudinal data for the free-flight-tunnel and Convair models are presented for a center-of-gravity position of 30.0 percent of the mean aerodynamic chord.

The static longitudinal stability and control characteristics of the free-flight-tunnel and Convair models are presented in figure 4. These data show that the lift-curve slopes, the maximum lift coefficient, and the drag coefficients were generally slightly higher for the free-flight-tunnel model. A comparison of the pitching-moment curves shows that the models had about the same static longitudinal stability -  $\frac{dC_m}{dC_L}$  and elevator effectiveness over the lift-coefficient range.

The leading-edge slats of figure 2 were used on the model because preliminary tests showed that they had a beneficial effect on the lateral stability characteristics at higher angles of attack. These slats were obviously not the optimum configuration for producing the most satisfactory longitudinal characteristics for the model investigated as shown by the data of figure 4. These data show that the slats decreased the lift-curve slope and maximum lift coefficient and reduced the longitudinal stability

at the higher angle of attack although the model was still stable over the angle-of-attack range. Brief flow studies made with a tuft probe showed that the slats interrupted the vortex flow from the wing and thereby tended to eliminate any favorable effect of the vortex flow on the lift characteristics of the wing at high angles of attack.

### Force Tests to Determine Lateral Stability

Force tests were made to determine the static lateral stability and control characteristics of the model with vertical tail off and on over a sideslip range from  $20^\circ$  to  $-20^\circ$  for angles of attack from  $0^\circ$  to  $35^\circ$ . These data were obtained at the same dynamic pressure and center-of-gravity location as for the longitudinal data. Presented for comparison with the free-flight-tunnel data are higher Reynolds number data obtained from tests conducted at Convair. These Convair data are presented for a center-of-gravity position of 27.5 percent of the mean aerodynamic chord.

Basic design.— The lateral stability characteristics of the free-flight-tunnel and Convair models in the basic configurations are presented in figures 5 and 6 with controls neutral. The data of figures 5 and 6 are summarized in figure 7 in terms of the directional-stability parameter  $C_{n\beta}$

and effective-dihedral parameter  $-C_{l\beta}$ . Since the data of figures 5 and 6 are nonlinear for some conditions, the data of figure 7 are presented at low angles of sideslip ( $\beta = \pm 2^\circ$ ) and high angles of sideslip ( $\beta = \pm 10^\circ$ ). The data of figure 5 show that the variation of the yawing-moment coefficient  $C_n$  and the rolling-moment coefficient  $C_l$  with angle of sideslip  $\beta$  is fairly linear up to an angle of attack of  $20^\circ$  for the model with vertical tail off and on. At an angle of attack of  $25^\circ$  the tail-off configuration shows a large increase in directional instability. This increase in negative slope of the yawing-moment curve for the tail-off configuration is also reflected in the data for the tail-on configuration at  $25^\circ$  angle of attack. In addition, at  $25^\circ$  angle of attack and higher the tail-on data show a sharp destabilizing break in the yawing-moment curve at sideslip angles greater than approximately  $\pm 2^\circ$  to  $\pm 5^\circ$ . A comparison of the data for the tail-off and tail-on configurations above  $20^\circ$  angle of attack shows that, for small angles of sideslip, the effectiveness of the vertical tail actually increases. This increase in effectiveness of the tail was probably caused by the tail being in a favorable region of sidewash from the wing-fuselage combination. At larger angles of sideslip the loss in effectiveness of the vertical tail was probably caused by the tail moving into an unfavorable region of the vortex flow from the wing-fuselage combination. An erratic variation of the rolling-moment curves also occurred at high angles of attack.

A comparison of the data of figure 6 shows that in general the Convair model had about the same variation in the yawing-moment and rolling-moment

curves as those for the free-flight-tunnel model. The nonlinearities in the data of figures 5 and 6 resulted in considerable differences in the directional-stability parameter  $C_{n\beta}$  and the effective-dihedral parameter  $-C_{l\beta}$  determined at low and high angles of sideslip. These differences are shown more clearly in the data of figure 7.

The data of figure 7 indicate that the free-flight-tunnel model had lower directional stability over the lift range than the Convair model, but that the two models became directionally unstable at about the same lift coefficient. The lower stability of the free-flight-tunnel model appears to be caused by the greater instability of the wing-fuselage combination. Because of the nonlinearities in the yawing-moment curves, the directional stability determined for  $\beta = \pm 10^\circ$  decreased to zero at about  $4^\circ$  angle of attack lower or 0.10 lift coefficient lower, than that for  $\beta = \pm 2^\circ$ .

The effective dihedral  $-C_{l\beta}$  was generally positive for both models over the lift-coefficient range with the free-flight-tunnel model having slightly higher values of  $-C_{l\beta}$  at the higher lift coefficients. At the stall the effective dihedral dropped to low positive or even negative values. At the higher angles of attack the effective dihedral for the free-flight-tunnel model was more positive at  $\beta = \pm 2^\circ$  than at  $\beta = \pm 10^\circ$ . Near the stall the effective dihedral of the Convair model became more negative at  $\beta = \pm 2^\circ$  than at  $\beta = \pm 10^\circ$ .

Modified design.- In an effort to obtain satisfactory static lateral stability characteristics at high angles of attack, force tests were made of the model with increased vertical-tail size (tails B and C) and with leading-edge slats (see fig. 2). All these data are presented for an elevon deflection of  $-15^\circ$  which corresponded approximately to the deflection needed to trim at high lift coefficients (see fig. 4). The data obtained in these tests are presented in figures 8 and 9. The data of figure 10 compare the lateral characteristics of the basic model with those of the modified model at angles of attack of  $25^\circ$  and  $30^\circ$ . The data of figures 8 and 9 are summarized in figure 11 in terms of the lateral-stability parameters  $C_{Y\beta}$ ,  $C_{n\beta}$ , and  $-C_{l\beta}$  for angles of sideslip of  $\pm 2^\circ$  and  $\pm 10^\circ$ .

A comparison of the data of figures 5 and 8 or 7 and 11 shows that the elevon deflection of  $-15^\circ$  had little effect on the directional stability characteristics. The deflection of the elevons did, however, increase the positive dihedral effect in the higher angle-of-attack range.

The data of figure 10 show that at an angle of attack of  $25^\circ$  increasing the size of the vertical tail (tail B or tail C) increased the directional stability, but the sharp destabilizing break in the yawing-moment-coefficient curve at moderate angles of sideslip obtained with the

basic design still occurred with either of the larger tails. The leading-edge slats produced a small increment in directional stability at low angles of sideslip and a very large increment in directional stability at high angles of sideslip so that the overall result was a fairly linear variation of the yawing-moment coefficient with angle of sideslip. This large increase in directional stability at high angles of sideslip is apparently associated with the change in vortex flow brought about by the addition of the slats. As previously mentioned, the slats interrupted the vortex flow from the wing at high angles of attack and thereby eliminated the unfavorable sidewash over the tail. The data of figure 10(b) show that the combination of tail B with the leading-edge slats provided positive static directional stability over the angle-of-sideslip range up to an angle of attack of  $30^\circ$ .

The summary data of figure 11 show the effects of the increased tail size and leading-edge slats more clearly. These data show that for low sideslip angles ( $\pm 2^\circ$ ) increasing the vertical-tail size increased the directional stability and increased the lift coefficient at which the directional stability became zero. At the stall, however, the model still became directionally unstable. For sideslip angles of  $\pm 10^\circ$ , tails B and C provided a smaller improvement in  $C_{n\beta}$  than at  $\pm 2^\circ$  sideslip angles.

At high angles of attack the addition of the leading-edge slats reduced the instability of the model at a given angle of attack but because of the adverse effect of the slats on the lift characteristics of the model the slats did not increase the lift coefficient at which the model became directionally unstable. Since the slats produced an approximately linear variation of the lateral derivatives with angle of sideslip, the slats-on data of figure 11 are essentially the same at either  $\pm 2^\circ$  sideslip or  $\pm 10^\circ$  sideslip.

A combination of the leading-edge slats and tail B produced the most satisfactory lateral stability characteristics for the configurations investigated (see fig. 11). This configuration resulted in the model being stable up to the stall even at the high angles of sideslip.

The effective dihedral  $-C_{l\beta}$  for the basic design was positive over most of the lift-coefficient range although there was some decrease in positive dihedral effect at the stall. The addition of the slats produced a large increase in  $-C_{l\beta}$  over the higher lift-coefficient range. At low angles of sideslip, tails B and C provided slightly higher  $-C_{l\beta}$  than tail A.

#### Force Tests to Determine Lateral Control.

The data presented in figure 12 show that the rolling-moment and yawing-moment coefficients produced by a given aileron deflection are

generally about the same for the free-flight-tunnel and Convair models except that the Convair model had slightly higher values of rolling moment and adverse yawing moment near the stall. The addition of slats to the free-flight-tunnel model did not greatly alter the aileron effectiveness of the model but gave slightly higher values of adverse yawing moment at the stall.

The results of tests to determine the rudder effectiveness of the free-flight-tunnel model indicate that the yawing moment produced by a rudder deflection of  $10^\circ$  was sufficient to balance out the maximum adverse yawing moment produced by  $\pm 15^\circ$  deflection of the ailerons (fig. 12).

#### Force Tests to Determine Rolling Derivatives

Rotary tests were made to determine the rolling derivatives of the model with elevons at  $0^\circ$  and  $-15^\circ$  with the basic vertical tail (tail A) on and off. All rotary tests were run at a dynamic pressure of 4.2 pounds per square foot which corresponds to an airspeed of approximately 59.0 feet per second at standard sea-level conditions and to an effective Reynolds number of 877,000 based on the mean aerodynamic chord of 2.32 feet.

The rotary-test data for the model presented in figure 13 show a decrease in the damping-in-roll parameter  $-C_{l_p}$  as the angle of attack increased. The yawing-moment-due-to-rolling parameter  $C_{n_p}$  for the complete model reached large negative values in the higher angle-of-attack range because of the large negative increment contributed by the vertical tail.

#### FLIGHT TESTS

Flight tests were made from a lift coefficient of about 0.50 through the stall to determine the dynamic stability and control characteristics of the model in its basic configuration and with increased tail size and leading-edge slats. All the flight tests were made at a center-of-gravity position of 30 percent of the mean aerodynamic chord. Only relatively low-altitude conditions were simulated and no attempt was made to determine the effect of freeing the controls.

Most of the flights were made at the light loading (table I) in order to minimize damage to the model in crackups, but a few flights were made with the model at the scaled-down normal gross weight and with approximately the correct scaled-down values of the radii of gyration of the full-scale airplane.

## FLIGHT-TEST RESULTS AND DISCUSSION

~~CONFIDENTIAL~~

## Longitudinal Stability and Control

Although the longitudinal characteristics of the model were considered to be generally satisfactory, some difficulty was encountered in flying the model in the high lift-coefficient range because of the large variation of drag with lift, which is generally a characteristic of low-aspect-ratio swept wings (ref. 4). This large variation of drag with lift caused large variations of the glide angle with lift coefficient and necessitated almost continuous corrections to tunnel angle and airspeed in order to maintain flight in the tunnel.

## Lateral Stability

Basic design.- The lateral (Dutch Roll) oscillations were well damped for all flight conditions. The directional stability, however, decreased with increasing angle of attack and at an angle of attack near the stall ( $\alpha = 25^\circ$ ) the model became directionally divergent. The model could be flown at this angle of attack as long as the pilot was able to keep the angle of sideslip small. It appeared, however, that once an angle of sideslip of approximately  $5^\circ$  was reached, the model could not be recovered and it diverged rapidly to larger angles of sideslip and snap-rolled violently into the tunnel wall. A typical flight record of the model at an angle of attack of  $25^\circ$  is shown in figure 14(a). This behavior is apparently similar to that of the Bell X-5 airplane which experienced a directional divergence in flight (see ref. 5). The directional divergence of the free-flight-tunnel model was evidently caused by the large values of static directional instability at the higher angles of attack. The increased rate of the divergence at the moderate and large angles of sideslip is attributed to the sharp destabilizing break in the yawing-moment curve which occurred at the higher angles of attack. Another factor which might have contributed to the directional divergence was the decrease in positive effective dihedral in the higher angle-of-attack range.

As flights were attempted at angles of attack above  $25^\circ$ , it became more difficult for the pilot to keep the model at small angles of sideslip and the divergence became more violent. By using almost continued control in an effort to keep the model from yawing, the pilot could sometimes maintain flight for fairly long periods of time at angles of attack of  $27^\circ$  or  $28^\circ$  but the model eventually diverged in sideslip and rolled off. Flights attempted at  $30^\circ$  angle of attack were very short because the model diverged soon after take-off. A flight record of the model at an angle of attack of approximately  $30^\circ$  is presented in figure 14(b). This particular record shows that the model sideslipped to an angle of about  $60^\circ$  and rolled to an angle of about  $80^\circ$  before crashing into the tunnel wall.

By increasing the rudder deflection of the model from  $\pm 10^\circ$  to  $\pm 25^\circ$  better control over the yawing motion of the model was obtained and with careful use of the controls the directional divergence could be delayed to a slightly higher angle of attack. More effective use of the rudder yawing moment could probably be obtained if the rudder was deflected independently, but even the maximum available yawing moment of the rudder would be insufficient to balance out the yawing moment due to sideslip at sideslip angles greater than approximately  $\pm 5^\circ$  at an angle of attack of  $30^\circ$ .

The slower yawing motions and independent rudder control of the full-scale airplane might enable the pilot to control the yawing motion fairly

well and prevent a divergence in most cases even at high angles of attack. The danger of a directional divergence will still be very real, however, since the airplane might inadvertently reach the divergent conditions if the pilot becomes engrossed in some action such as an evasive maneuver in combat.

Modified design.- Increasing the size of the vertical tail by 40 percent (tail B) or by as much as 80 percent (tail C) did not eliminate the directional divergence but did increase the angle of attack at which the divergence occurred. Satisfactory flights were obtained up to about  $33^\circ$  angle of attack with either tail and it appeared that tail C was only slightly better than tail B. A record of a satisfactory flight of the model with tail C is presented in figure 14(c) for an angle of attack of the model of approximately  $30^\circ$ . When flights were attempted at an angle of attack of about  $33^\circ$  or higher the model diverged in sideslip with either tail B or tail C. The behavior of the model with increased tail size at  $33^\circ$  angle of attack was similar to that of the basic model at  $25^\circ$  angle of attack. A flight record showing a directional divergence of the model with tail C is presented in figure 14(d) for an angle of attack of the model of approximately  $33^\circ$ .

The addition of the slats increased the angle of attack at which the model became directionally divergent but the slats were not nearly as effective in eliminating the divergence as the increase in vertical-tail size. Satisfactory flights of the model with slats were obtained up to angles of attack of about  $28^\circ$  to  $30^\circ$ . At angles of attack of  $30^\circ$  and higher the model was directionally divergent. The behavior of the model with slats at  $30^\circ$  angle of attack (fig. 14(e)) was similar to that of the basic model at  $25^\circ$  angle of attack (fig. 14(a)). The difference in flight behavior of the model with and without slats can be explained by the static data of figures 10 and 11. The slats eliminated the sharp destabilizing break in the yawing-moment curve at high angles of attack mainly by eliminating the unfavorable sidewash over the vertical tail when the model reached moderate and large sideslip angles. The slats also slightly reduced the directional instability at low sideslip angles and provided a large increase in positive dihedral effect at the higher angles of attack. Previous experimental and theoretical work has indicated that an increase in  $-C_{l\beta}$  might tend to eliminate the directional divergence or increase the angle of attack at which the directional divergence occurs.

The use of leading-edge slats in combination with increased tail size (tail B) provided satisfactory directional stability characteristics through the stall and there was no evidence of a directional divergence. At the stall the model settled gently to the tunnel floor with very little rolling or yawing motion. Flight records of the model with these modifications are presented in figures 14(f) and 14(g) for angles of attack of  $30^\circ$  and  $33^\circ$ . The satisfactory behavior of the model in this configuration can be explained by the static data of figures 10 and 11

which show that  $C_{n\beta}$  remained positive through the stall at both  $\pm 2^\circ$  or  $\pm 10^\circ$  angles of sideslip.

### Lateral Control

The lateral control characteristics of the basic and modified configurations were considered satisfactory over the lift-coefficient range investigated. Although the control characteristics could not be evaluated through the stall for the basic configuration, it is believed that they would be similar to those of the model with slats and increased tail size since the static data of figure 12 show that there is no appreciable difference in the control effectiveness of these two configurations. In flights near the stall with slats and increased tail size, some adverse sideslip with ailerons alone was obtained because of the adverse yawing moments due to aileron deflections (fig. 12) and the adverse yawing moments due to rolling (fig. 13). This adverse sideslipping was eliminated, however, by using the rudder in combination with the ailerons for coordinated control. In the higher angle-of-attack range there was no large decrease in lateral control effectiveness and the model was controlled satisfactorily through the stall.

As previously pointed out, full-scale flight tests of airplanes which have high yawing inertia and low rolling inertia similar to that of the YF-102 indicated more severe adverse sideslip characteristics than were demonstrated by models of these airplanes in the free-flight tunnel. It is expected, therefore, that the adverse sideslipping behavior of the full-scale airplane may be objectionable at the high angles of attack.

### CONCLUSIONS

The following conclusions were drawn from the results of the free-flight-tunnel stability and control investigation on a 1/10-scale model of the Convair YF-102 airplane. The model was flown over a lift-coefficient range from 0.5 to the stall in its basic configuration and with several modifications involving leading-edge slats and an increase in vertical-tail size. Only relatively low-altitude conditions were simulated and no attempt was made to determine the effect of freeing the controls.

1. The longitudinal stability characteristics were considered satisfactory for the basic and modified configurations over the speed range investigated.

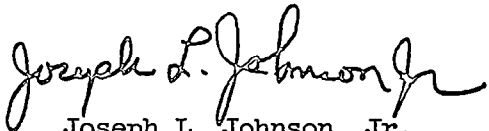
2. The lateral stability characteristics were considered satisfactory for the basic configuration over the speed range investigated except near

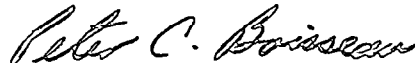
the stall where large values of static directional instability caused the model to be directionally divergent.

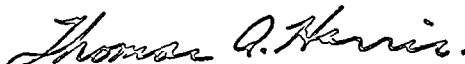
3. The addition of leading-edge slats or an 80-percent increase in vertical-tail area increased the angle of attack at which the model became directionally divergent. The use of leading-edge slats in combination with a 40-percent increase in vertical-tail area eliminated the directional divergence and provided satisfactory lateral stability characteristics through the stall.

4. The longitudinal and lateral control characteristics were generally satisfactory. Although the adverse sideslip characteristics for the model were considered satisfactory over the angle-of-attack range, analysis indicates that the adverse sideslip characteristics of the airplane may be objectionable at high angles of attack.

Langley Aeronautical Laboratory,  
National Advisory Committee for Aeronautics,  
Langley Field, Va., November 18, 1953.

  
Joseph L. Johnson, Jr.  
Aeronautical Research Scientist

  
Peter C. Boisseau  
Aeronautical Research Scientist

Approved:   
Thomas A. Harris  
Chief of Stability Research Division

mhg

## REFERENCES

1. Shortal, Joseph A., and Osterhout, Clayton J.: Preliminary Stability and Control Tests in the NACA Free-Flight Wind Tunnel and Correlation With Full-Scale Flight Tests. NACA TN 810, 1941.
2. Stone, Ralph W., Jr., Burk, Sanger M., Jr., and Bihrlé, William, Jr.: The Aerodynamic Forces and Moments on a 1/10-Scale Model of a Fighter Airplane in Spinning Attitudes as Measured on a Rotary Balance in the Langley 20-Foot Free-Spinning Tunnel. NACA TN 2181, 1950.
3. Werner, N. M.: Low Speed Wind Tunnel Tests of Various Vertical Tails on a 1/10 Scale Model of the F-102 Airplane. Rep. No. CVAL 101, Consolidated Vultee Aircraft Corp., Feb. 12, 1952.
4. McKinney, Marion O., Jr., and Drake, Hubert M.: Flight Characteristics at Low Speed of Delta-Wing Models. NACA RM L7K07, 1948.
5. Finch, Thomas W., and Walker, Joseph A.: Static Longitudinal Stability of the Bell X-5 Research Airplane With 59° Sweepback. NACA RM L53A09b, 1953.

TABLE I

## MASS AND DIMENSIONAL CHARACTERISTICS OF THE CONVAIR YF-102

## AIRPLANE AND SCALED-UP CHARACTERISTICS OF THE

## 1/10-SCALE MODEL TESTED IN THE

## LANGLEY FREE-FLIGHT TUNNEL

	Scaled-up		Full-scaled fighter at normal gross weight
	Light	Heavy	
Weight, lb . . . . .	14,570	22,890	22,890
Wing loading, W/S, lb/sq ft . . . . .	22.0	34.52	34.52
Relative density factor, $\mu_b$ . . . . .	7.53	11.81	11.81
Moments of Inertia:			
$I_X$ , slug-ft <sup>2</sup> . . . . .	13,900	13,900	13,627
$I_Y$ , slug-ft <sup>2</sup> . . . . .	84,500	84,500	89,357
$I_Z$ , slug-ft <sup>2</sup> . . . . .	87,400	87,400	99,635
Ratio of radius of gyration to wing span:			
$k_X/b$ . . . . .	0.145	0.116	0.1145
$k_Y/b$ . . . . .	0.358	0.286	0.2938
$k_Z/b$ . . . . .	0.364	0.291	0.3105
Wing:			
Airfoil . . . . .	NACA 0004-65 modified		
Area, sq ft . . . . .	661.50		
Span, ft . . . . .	38.13		
Aspect ratio . . . . .	2.198		
Root chord, ft . . . . .	34.69		
Tip chord, ft . . . . .	0		
$\bar{c}$ , ft . . . . .	23.22		
Longitudinal distance from leading-edge root chord			
to leading edge of $\bar{c}$ , ft . . . . .	11.01		
Sweepback of leading edge, deg . . . . .	60		
Sweepforward of trailing edge, deg . . . . .	5		
Dihedral, deg . . . . .	0		
Incidence, deg . . . . .	0		
Slats:			
Span, percent wing span (two) . . . . .	31.7		
Chord, ft . . . . .	1.36		

~~CONFIDENTIAL~~

TABLE I.- Concluded

## MASS AND DIMENSIONAL CHARACTERISTICS OF THE CONVAIR YF-102

## AIRPLANE AND SCALED-UP CHARACTERISTICS OF THE

## 1/10-SCALE MODEL TESTED IN THE

## LANGLEY FREE-FLIGHT TUNNEL

## Elevons:

Area behind hinge line, percent wing area (two)	10.12
Span, percent wing span (two)	69.0
Chord, parallel to fuselage reference axis, ft	3.02

## Vertical tail A (basic tail):

Airfoil section	NACA 0004-65 modified
Area, sq ft	67.0
Span, ft	11.35
Aspect ratio	1.93

## Vertical tail B:

Area, sq ft	93.0
Span, ft	13.80
Aspect ratio	2.05

## Vertical tail C:

Area, sq ft	117.0
Span, ft	13.80
Aspect ratio	1.63

## Rudder (same for tails A, B, and C):

Area, sq ft	12.65
Span, ft	5.72
Root chord, ft	2.1
Tip chord, ft	1.6

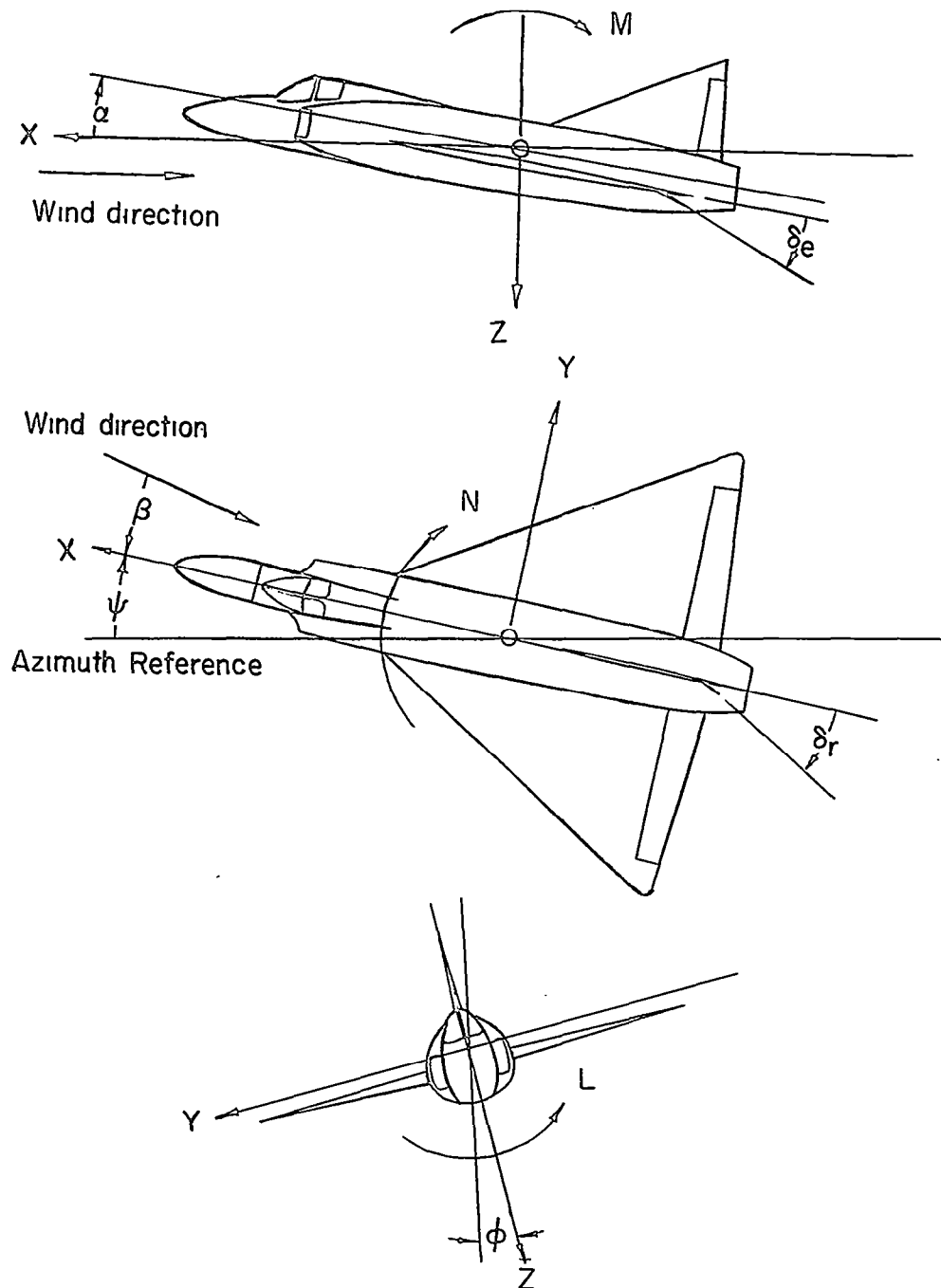


Figure 1.- The stability system of axes. Arrows indicate positive directions of moments, forces, and angles. This system of axes is defined as an orthogonal system having the origin at the center of gravity and in which the  $Z$ -axis is in the plane of symmetry and perpendicular to the relative wind, the  $X$ -axis is in the plane of symmetry and perpendicular to the  $Z$ -axis, and the  $Y$ -axis is perpendicular to the plane of symmetry. At a constant angle of attack, these axes are fixed in the airplane.



~~CONFIDENTIAL~~

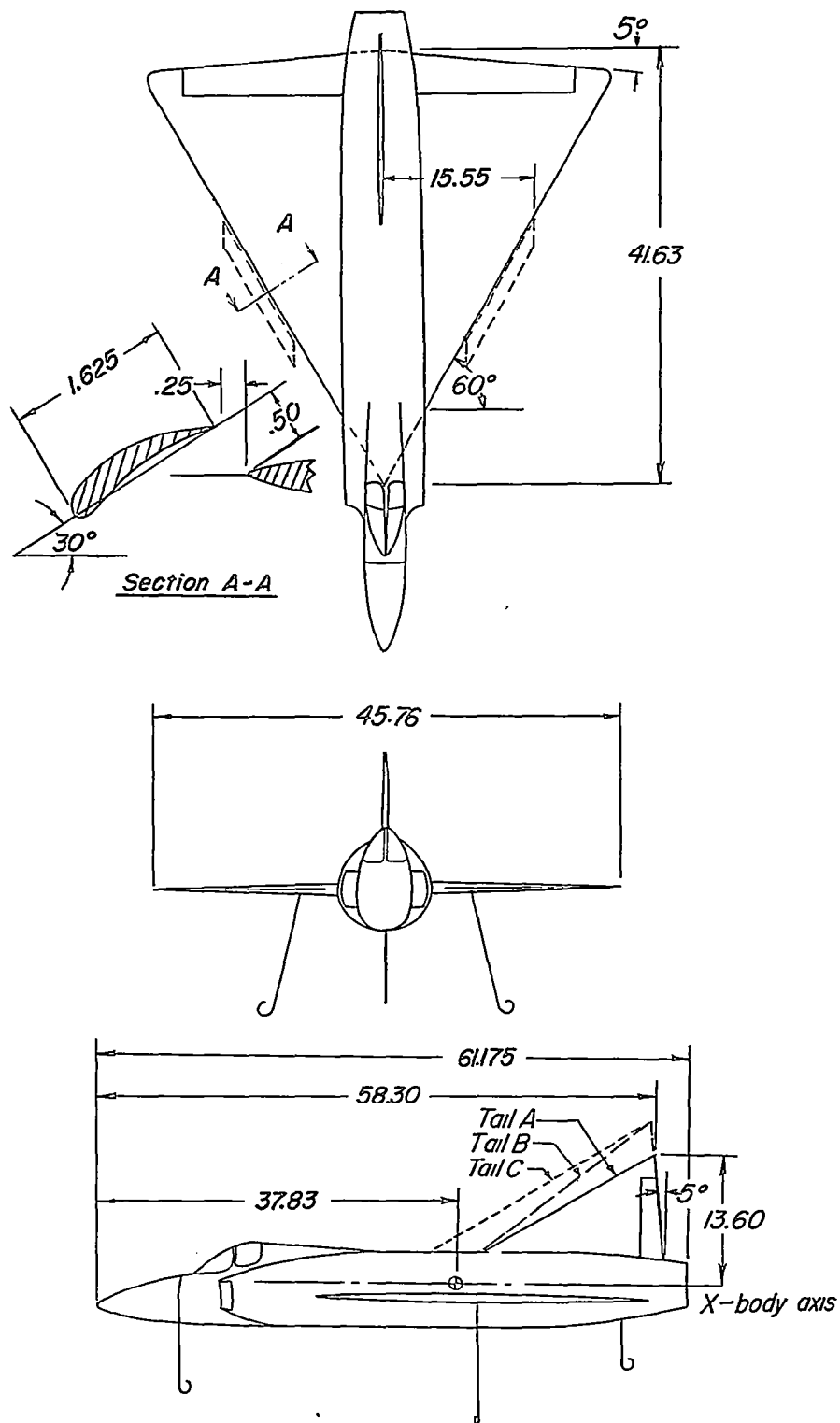
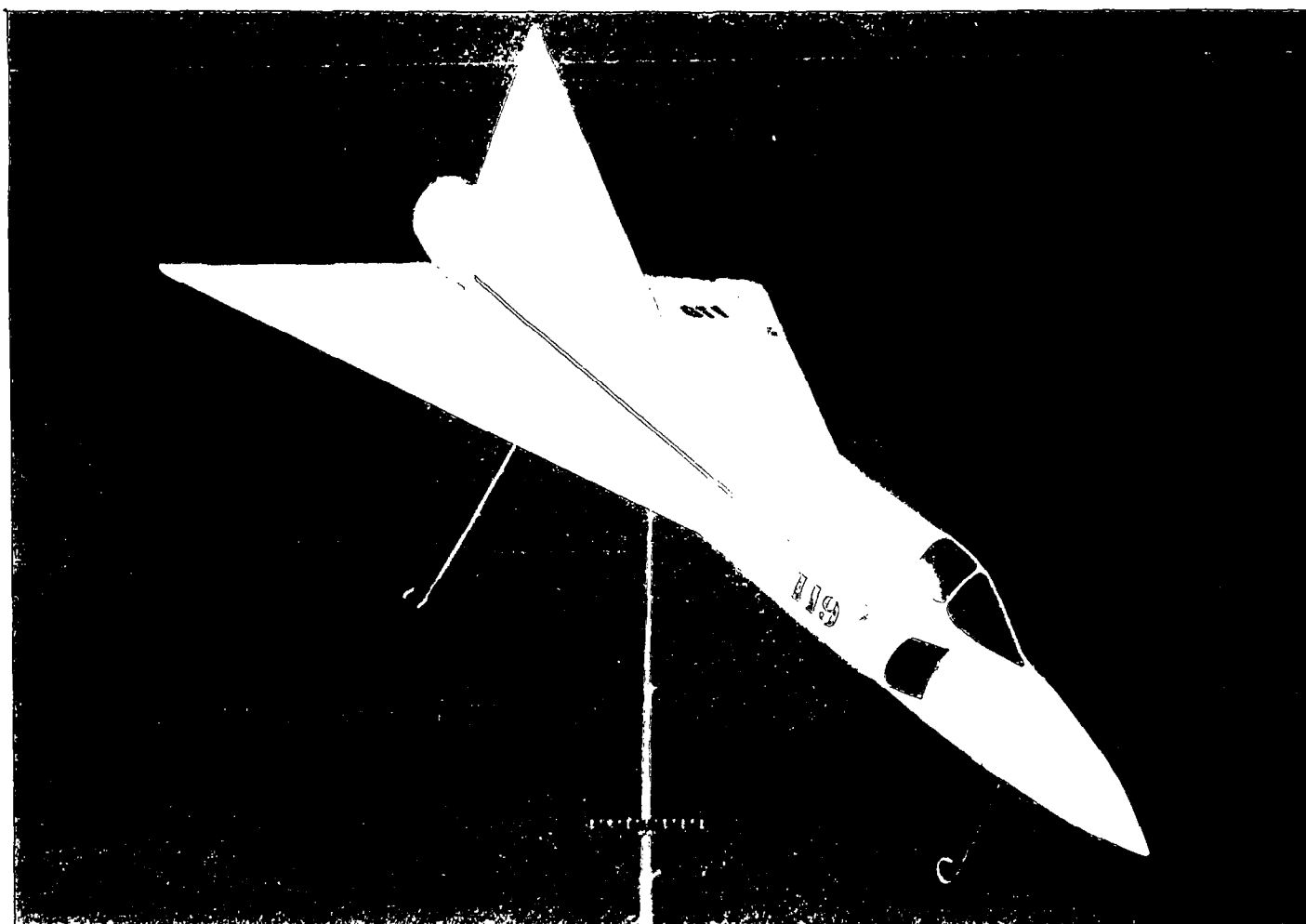


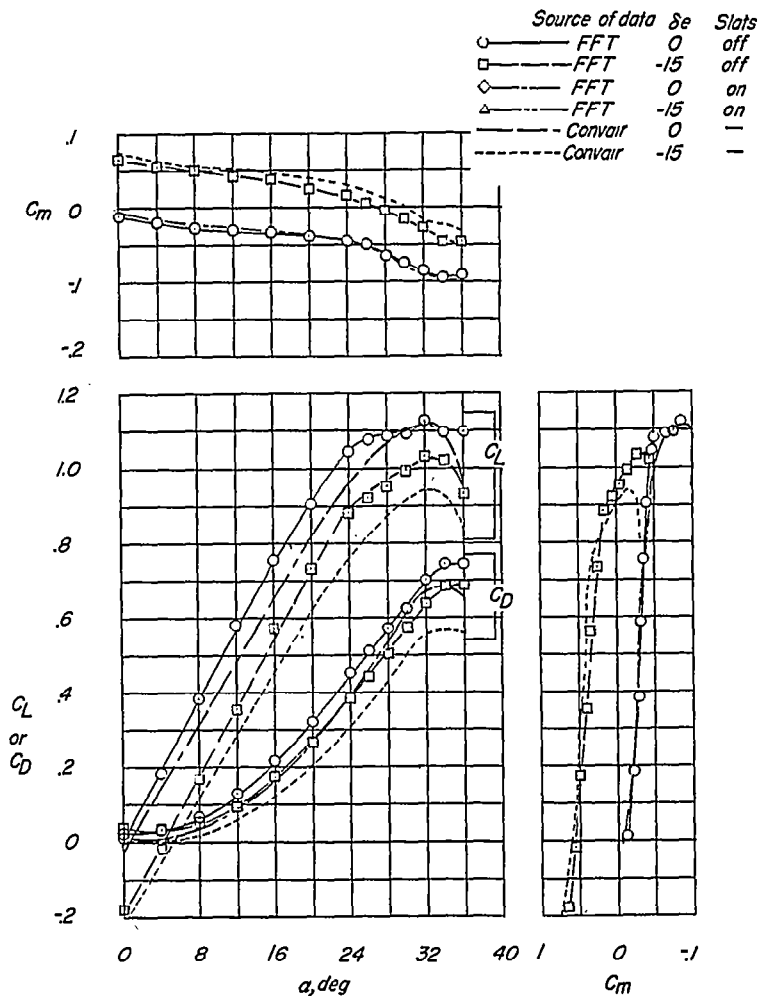
Figure 2.- Three-view drawing of a 1/10-scale model of the Convair YF-102 airplane tested in the Langley free-flight tunnel. All dimensions are in inches.

~~CONFIDENTIAL~~

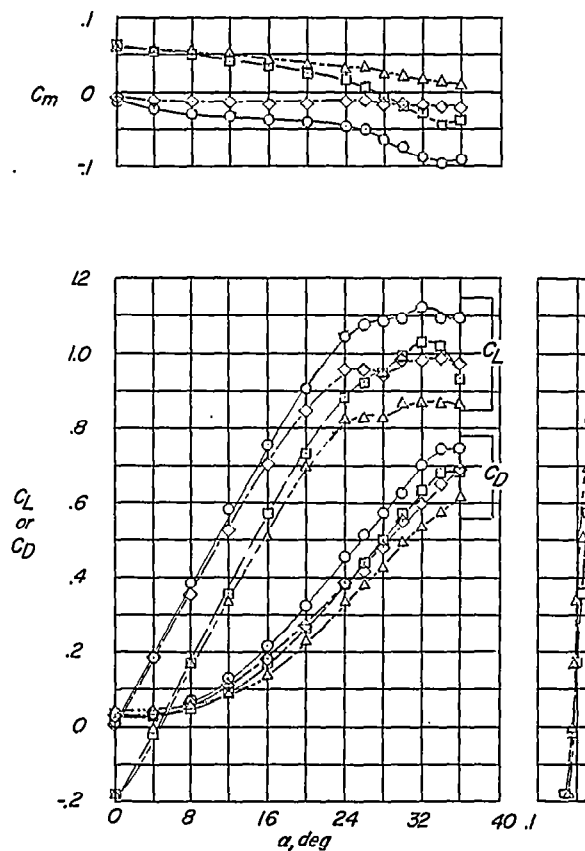


L-77848

Figure 3.- Photograph of 1/10-scale model of the Convair YF-102 airplane tested in the Langley free-flight tunnel. Air scoops closed.



(a) Comparison of free-flight tunnel and Convair data.

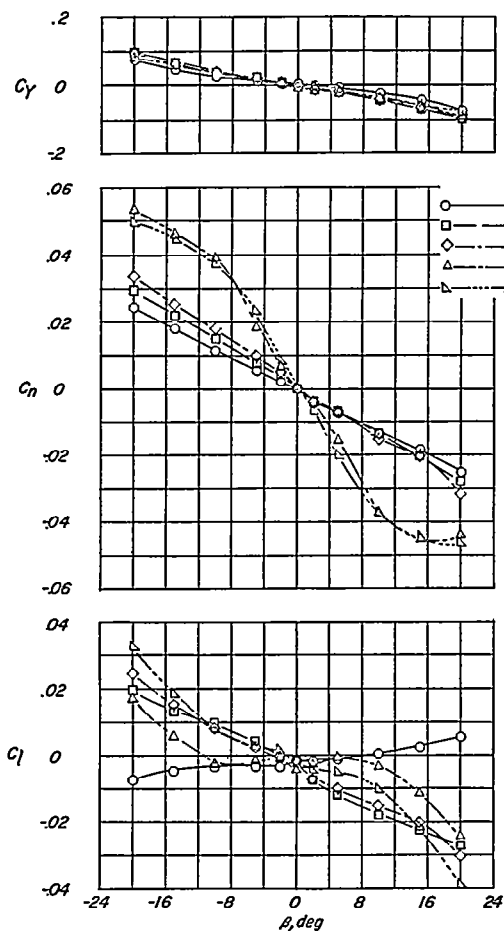
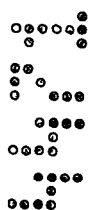


(b) Effect of leading-edge slats on the free-flight model.

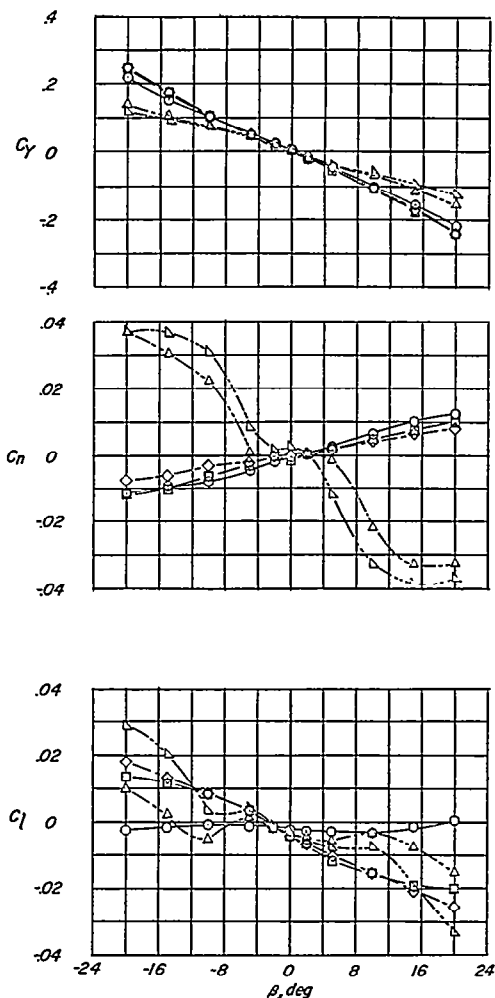
Figure 4.- Aerodynamic characteristics of models of the YF-102 airplane tested in the Langley free-flight tunnel and by Convair. Tail A.



~~CONFIDENTIAL~~



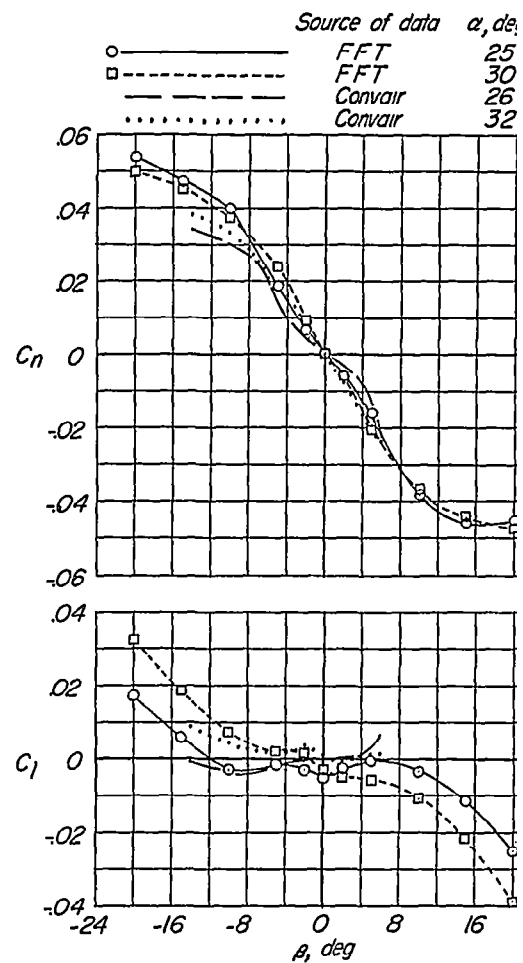
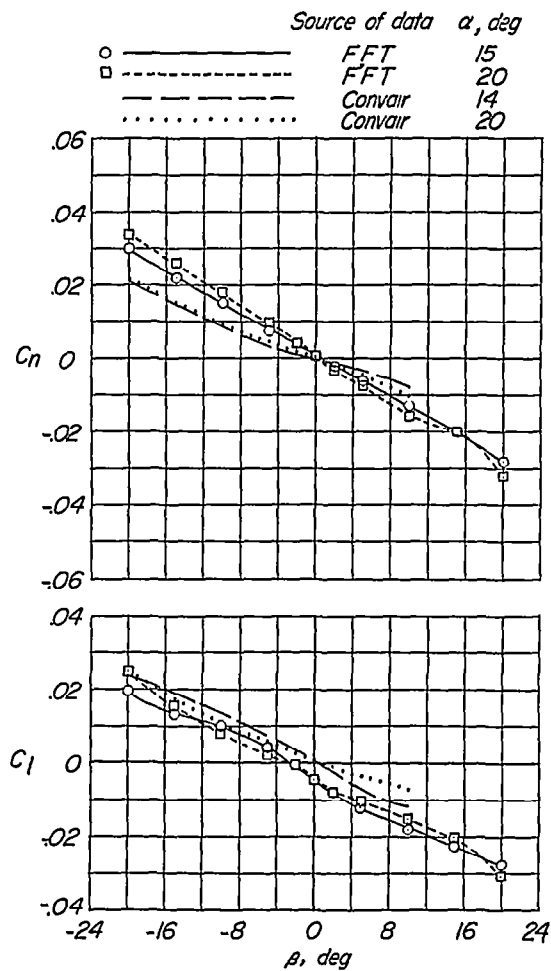
(a) Tail off.



(b) Tail A.

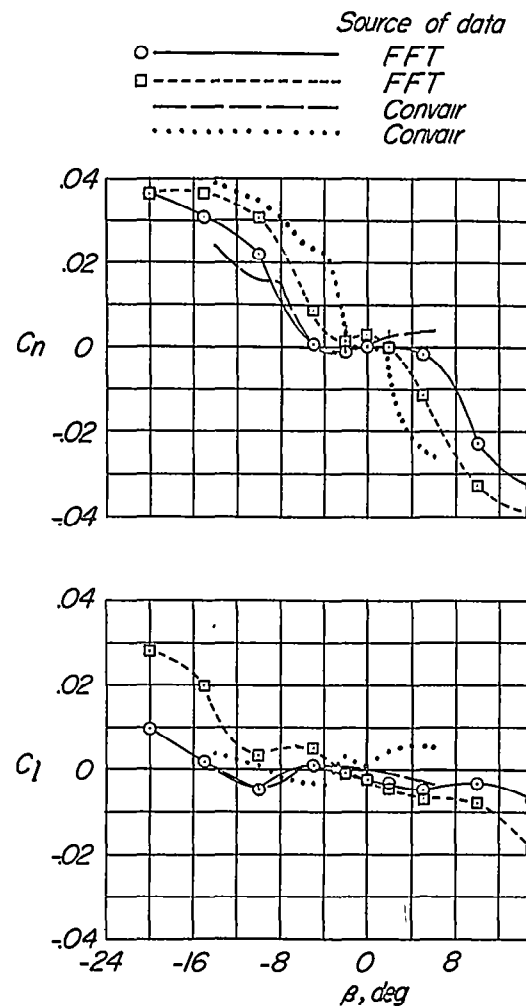
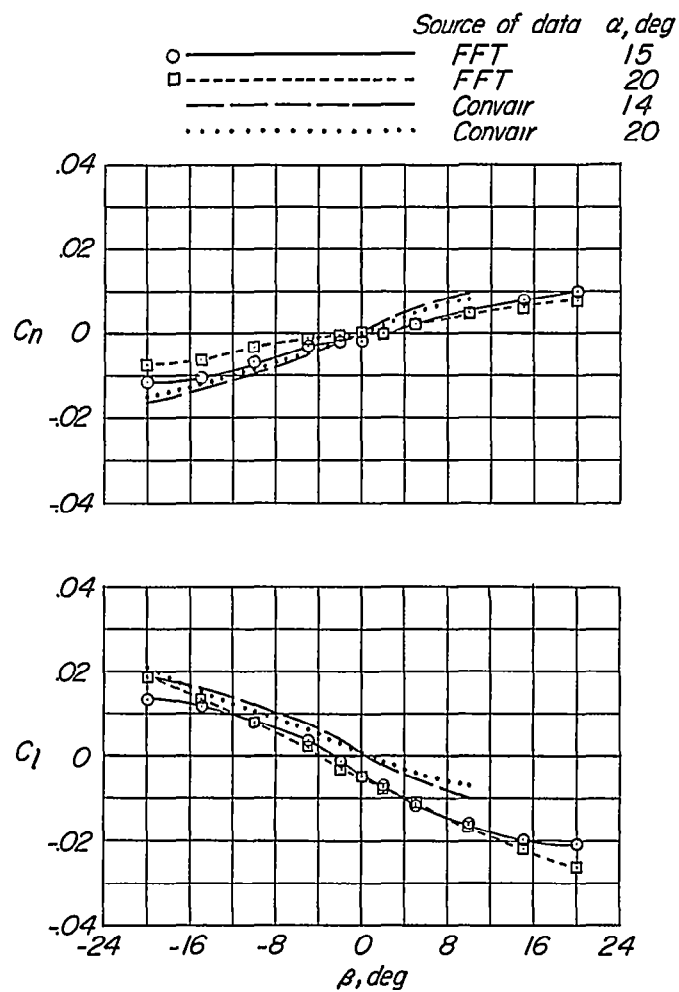
Figure 5.- Lateral characteristics of the model tested in the Langley free-flight tunnel.  $\delta_e' = 0^\circ$ .

~~CONFIDENTIAL~~



(a) Tail off.

Figure 6.- Comparison of the lateral stability characteristics of the models tested in the Langley free-flight tunnel and by Convair.  
 $\delta_e = 0^\circ$ .



(b) Tail A.

Figure 6.- Concluded.

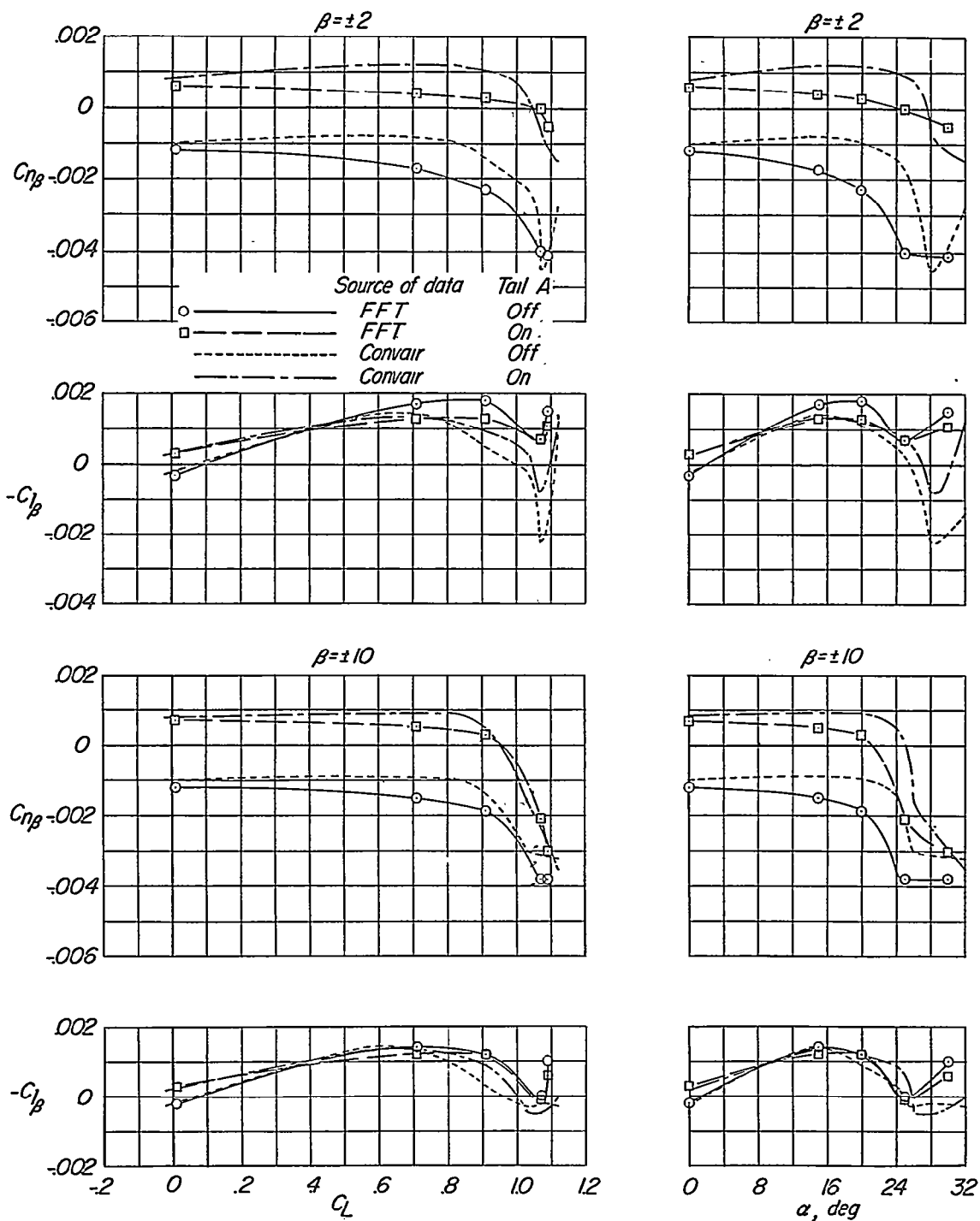
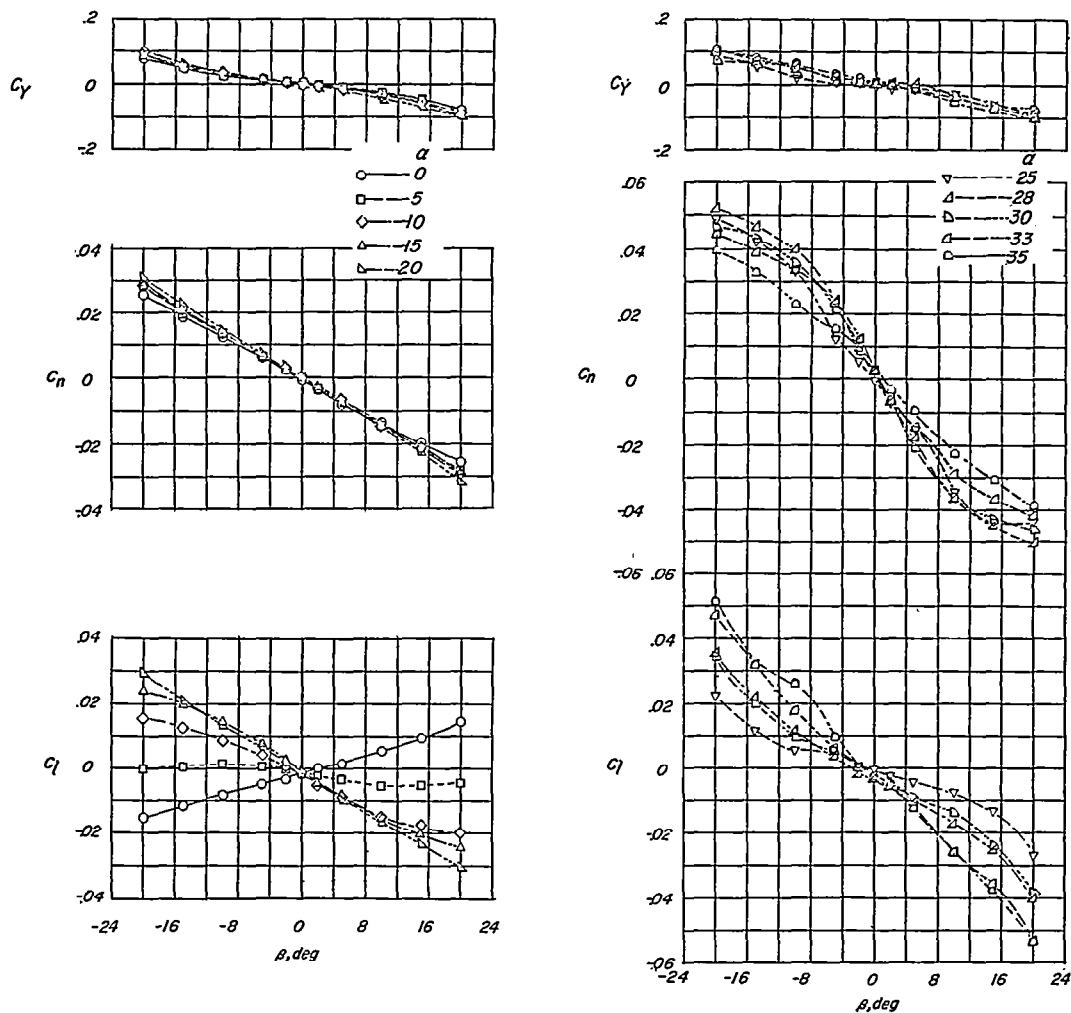
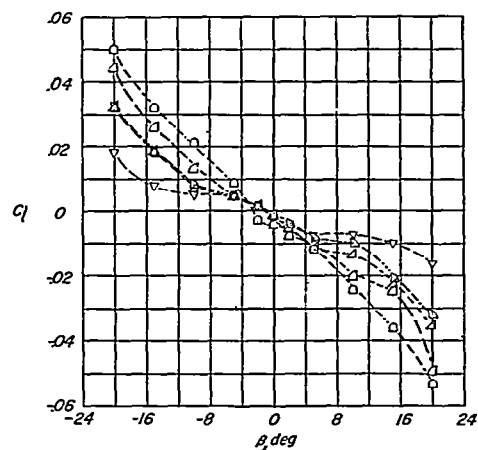
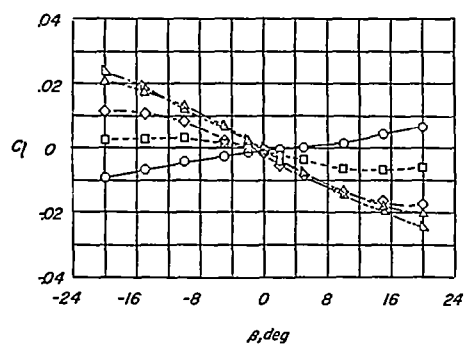
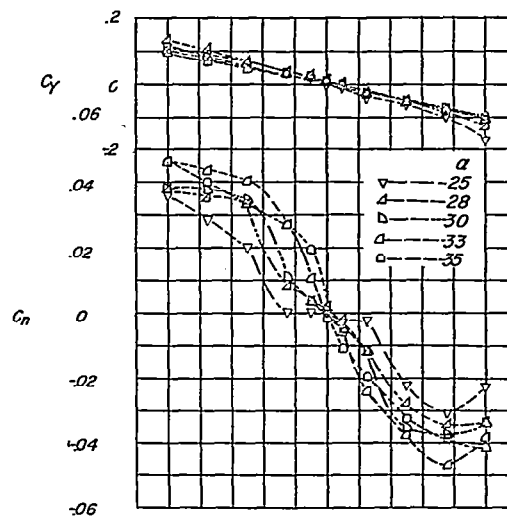
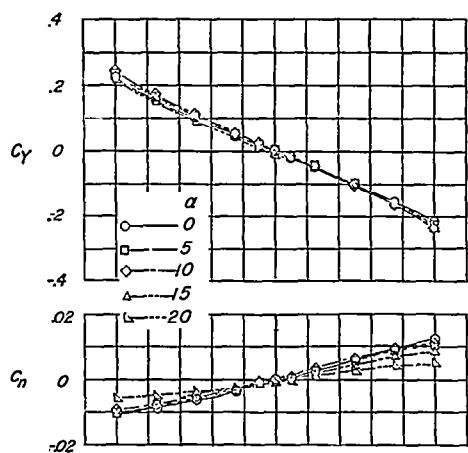


Figure 7.- Lateral-stability parameters of the models tested in the Langley free-flight tunnel and by Convair.  $\delta_e = 0^\circ$ .



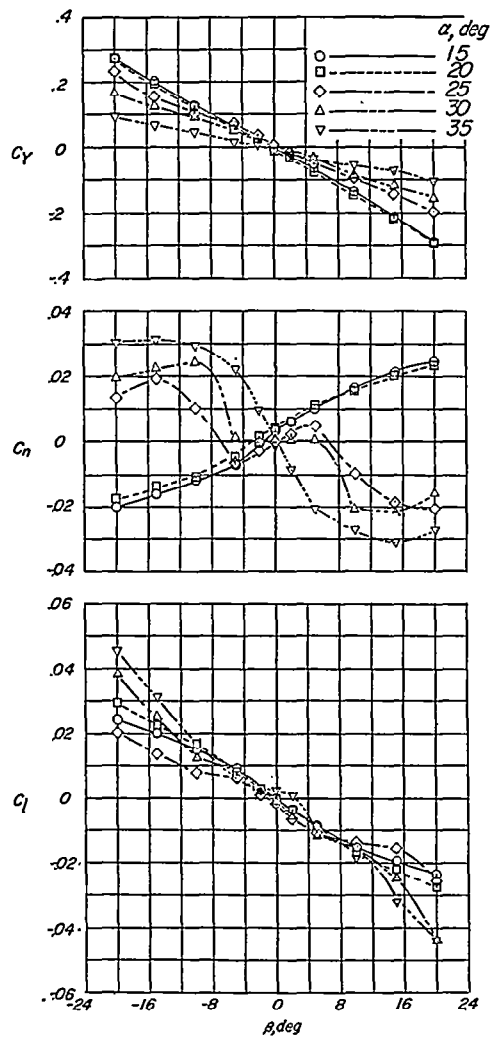
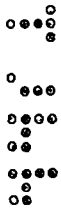
(a) Tail off.

Figure 8.- Lateral characteristics of the model tested in the Langley free-flight tunnel.  $\delta_e = -15^\circ$ .

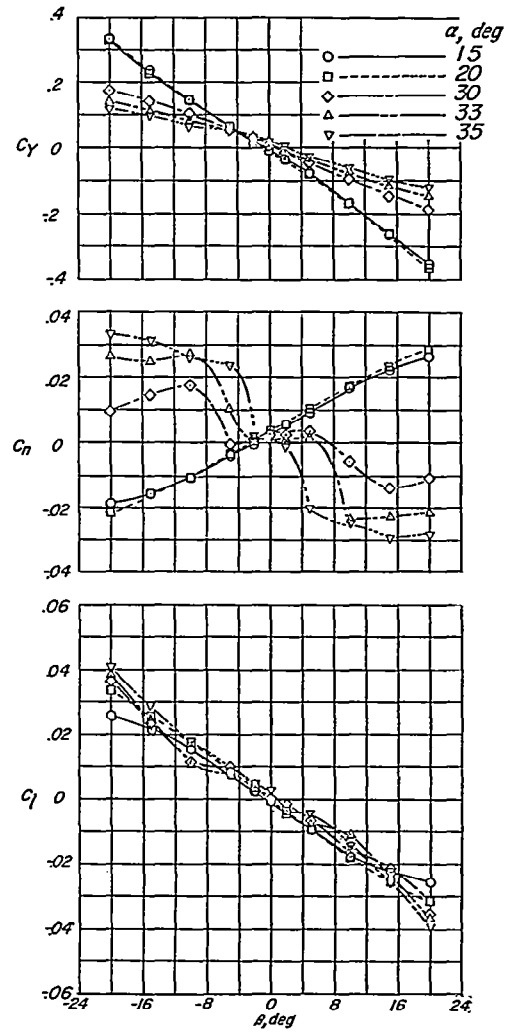


(b) Tail A.

Figure 8.- Continued.

~~CONFIDENTIAL~~

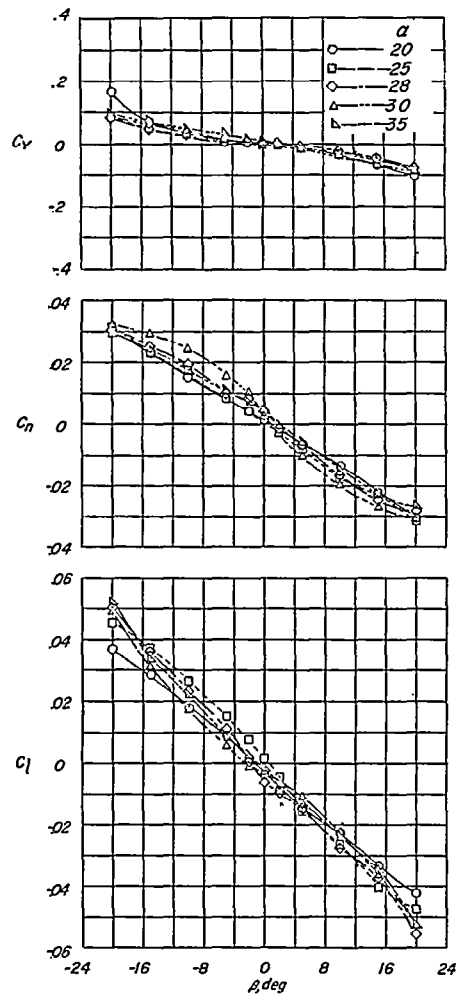
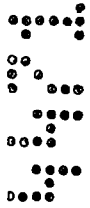
(c) Tail B.



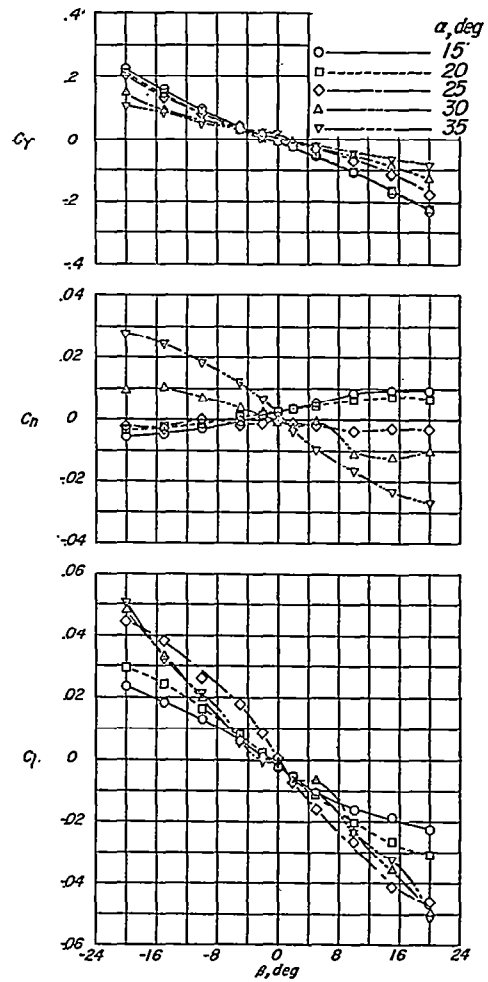
(d) Tail C.

Figure 8.- Concluded.

~~CONFIDENTIAL~~

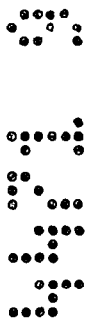
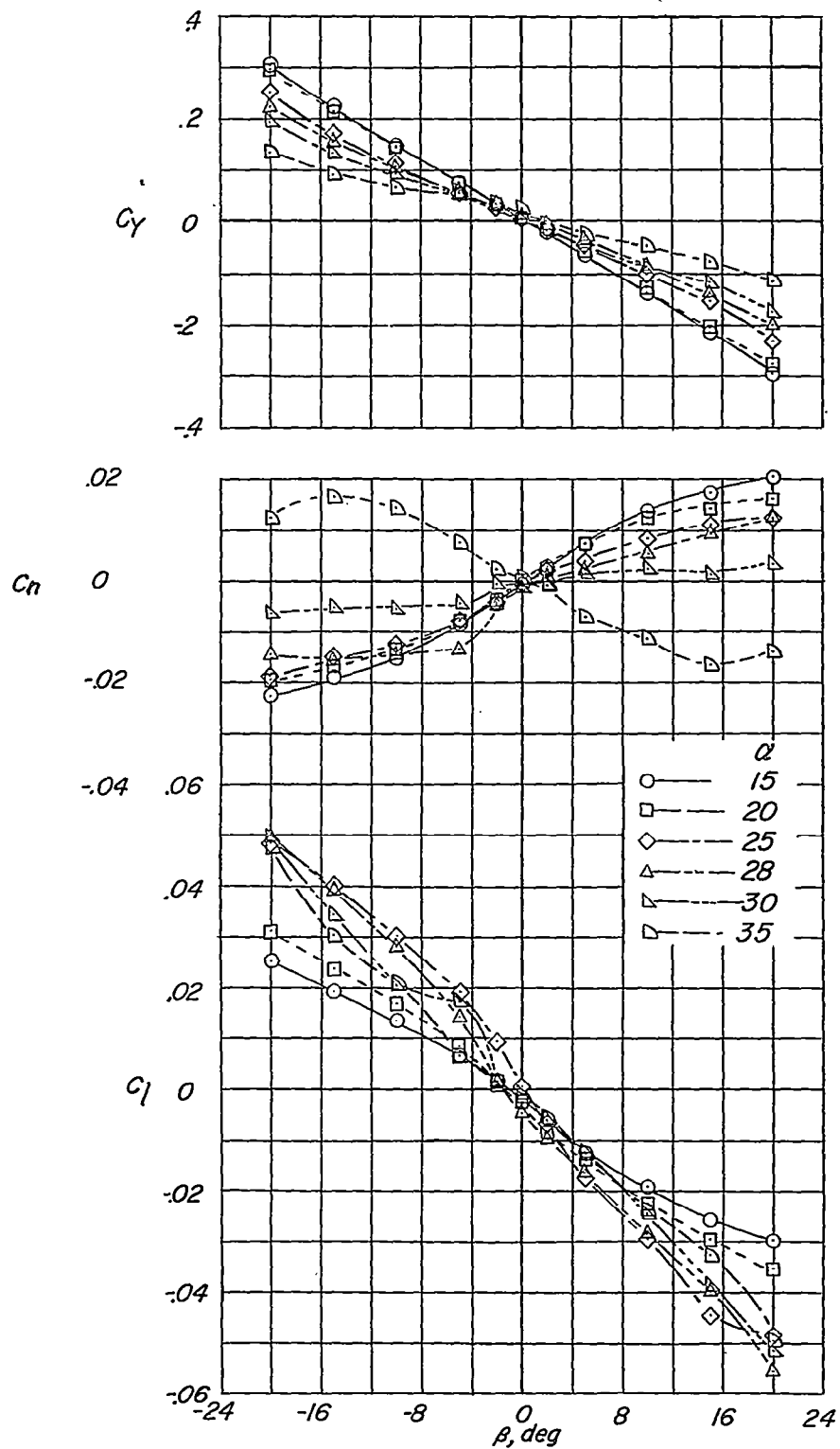


(a) Tail off.



(b) Tail A.

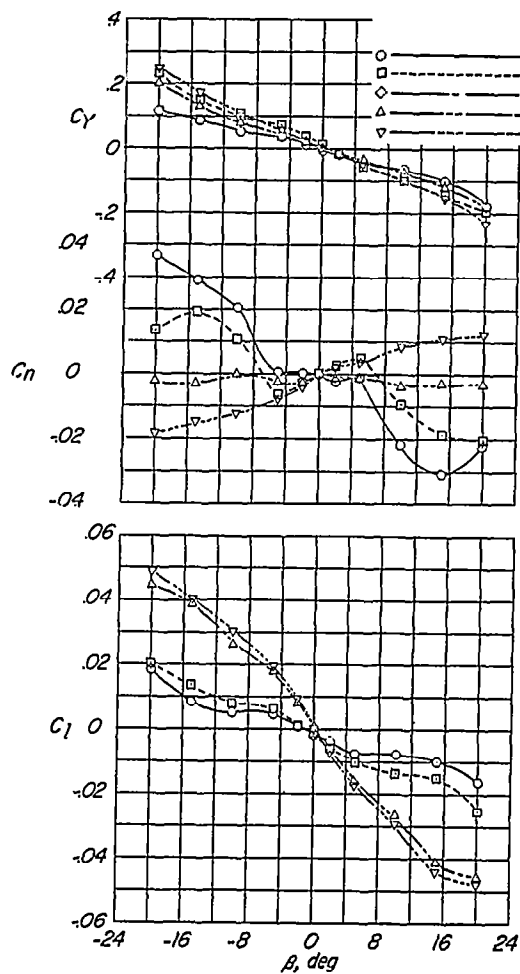
Figure 9.- Lateral characteristics of the Langley free-flight-tunnel model with leading-edge slats.  $\delta_e = -15^\circ$ .

~~CONFIDENTIAL~~

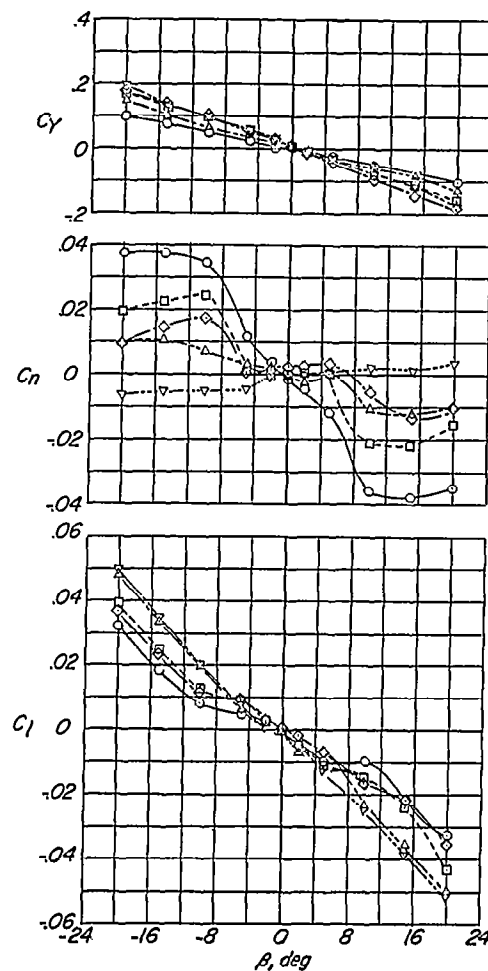
(c) Tail B.

Figure 9.- Concluded.

~~CONFIDENTIAL~~



(a)  $\alpha = 25^\circ$ .



(b)  $\alpha = 30^\circ$ .

Figure 10.- Comparison of the effects of several modifications on the lateral characteristics of the model tested in the Langley free-flight tunnel.  $\delta_e = -15^\circ$ .

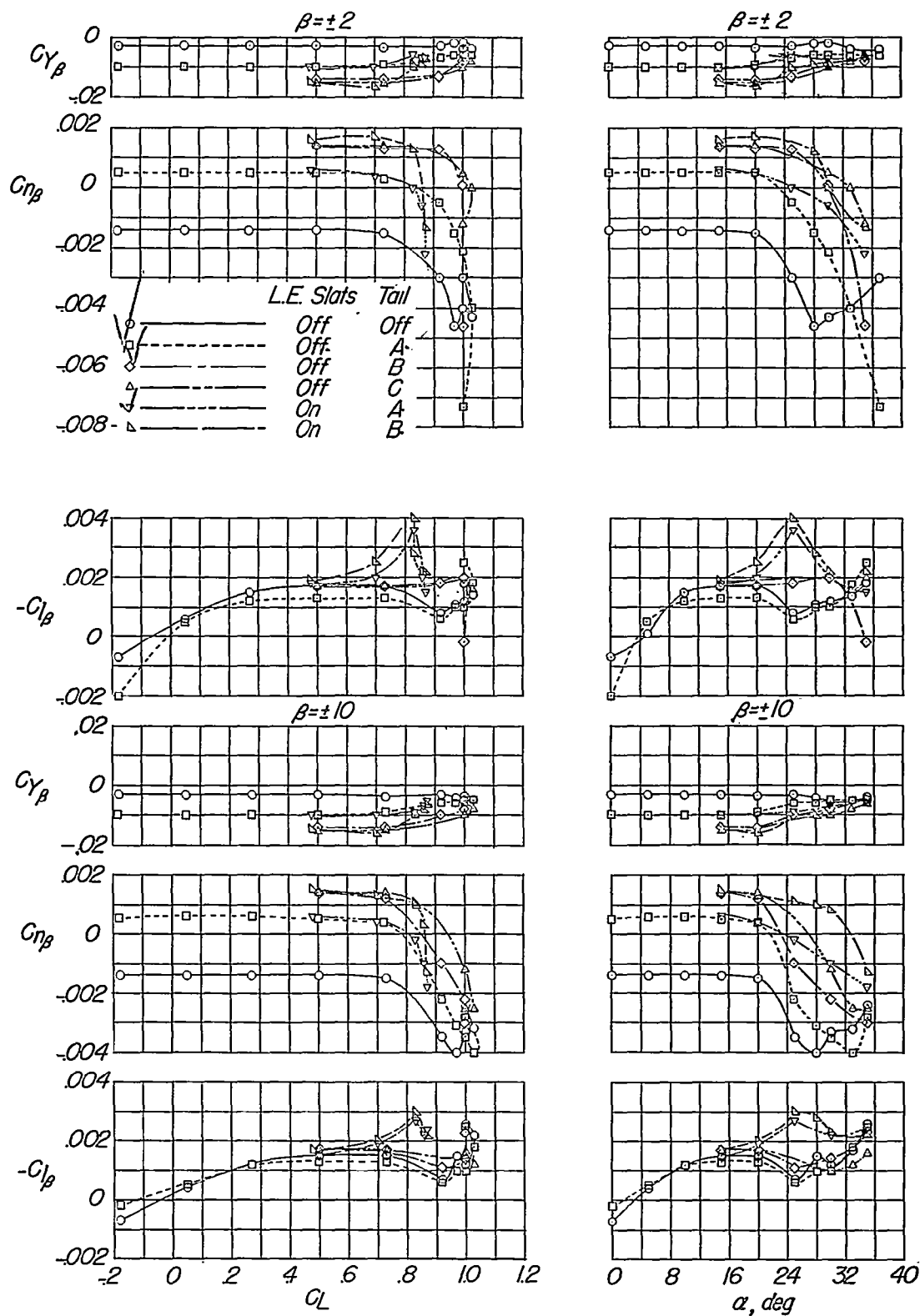
~~CONFIDENTIAL~~

Figure 11.- Lateral-stability parameters of the model tested in the Langley free-flight tunnel.  $\delta_c = -15^\circ$ .

~~CONFIDENTIAL~~

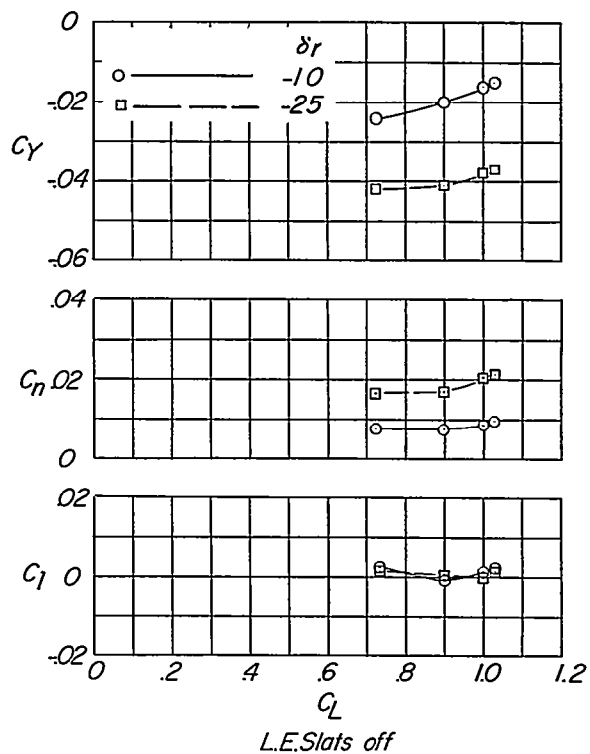
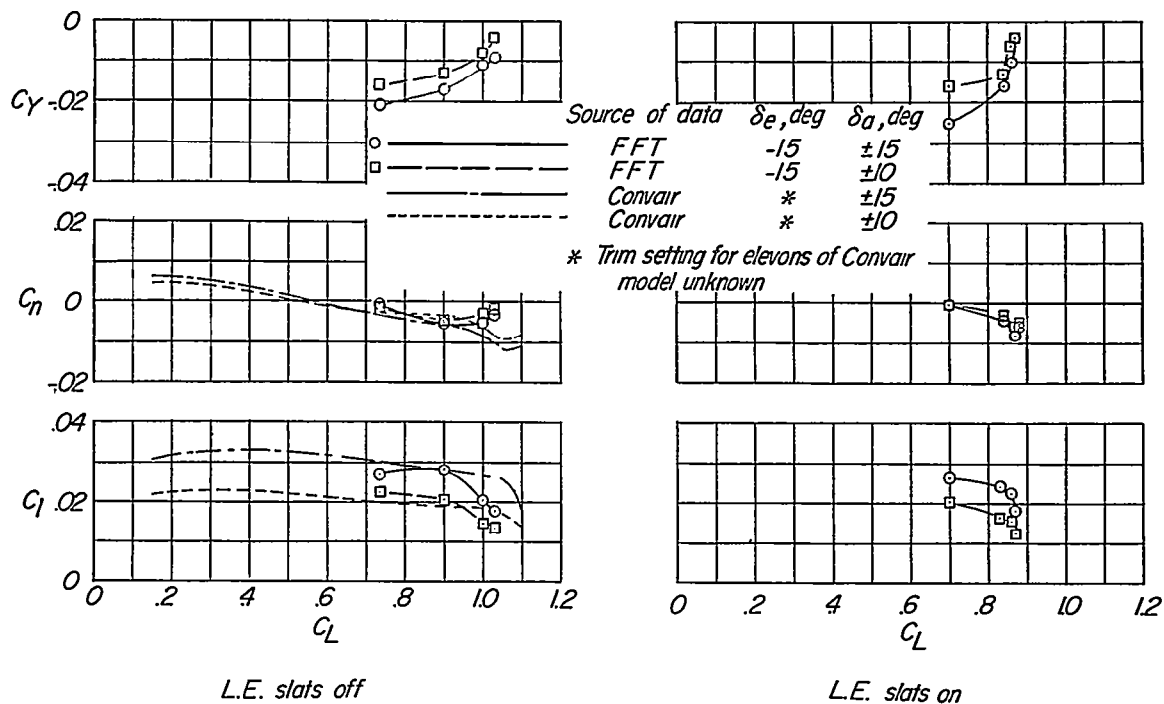
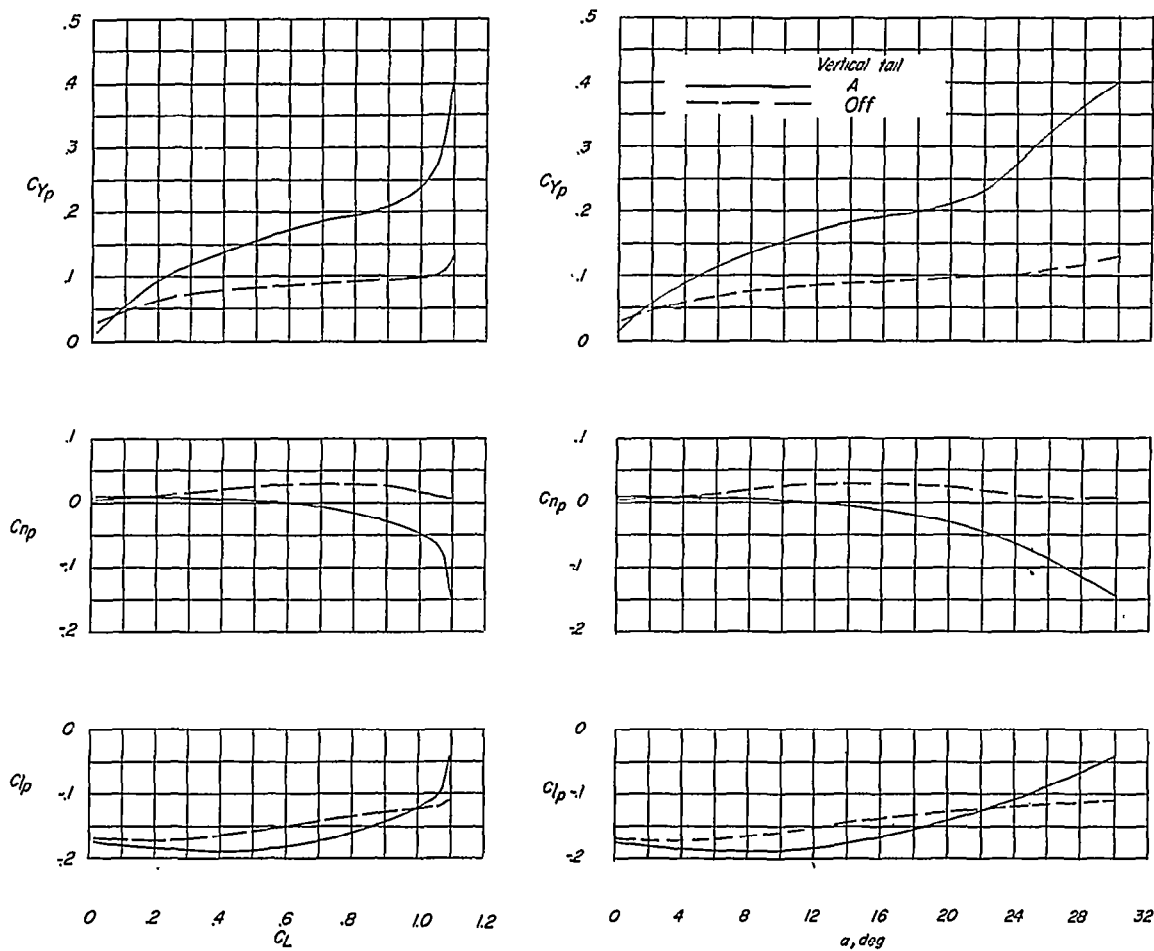


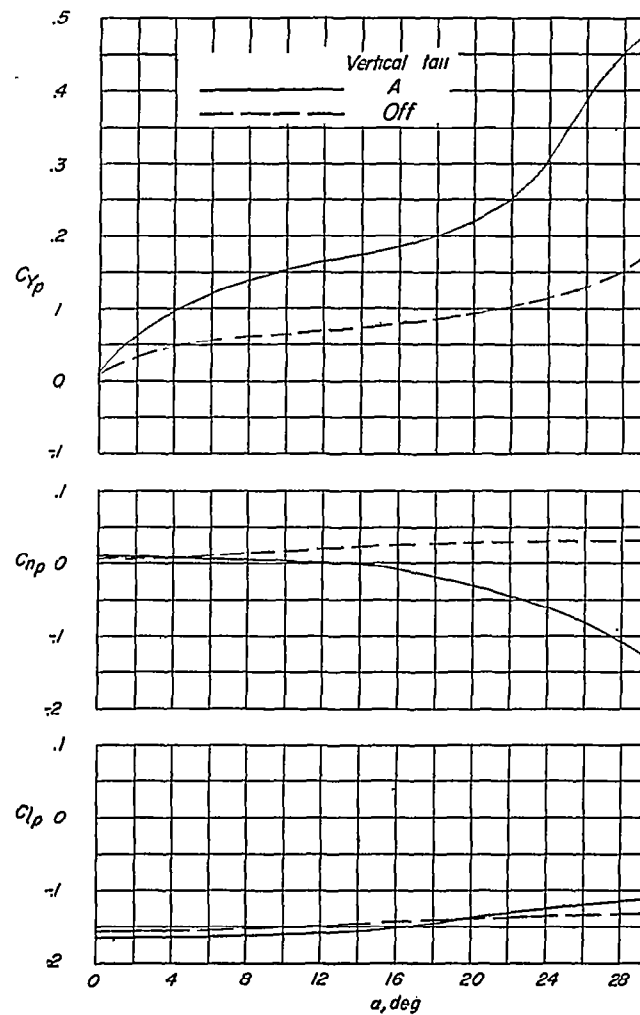
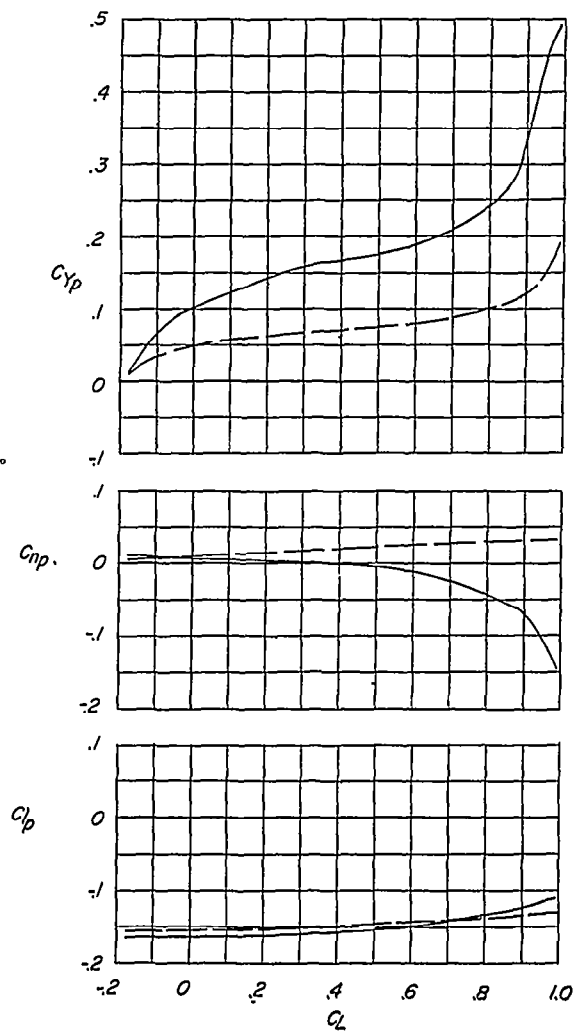
Figure 12.- Aileron and rudder effectiveness of the model tested in the Langley free-flight tunnel and aileron effectiveness of the model tested by Convair.  $\delta_e = -15^\circ$ ; tail A.

60  
50  
40  
30  
20  
10  
0



(a)  $\delta_e = 0^\circ$ .

Figure 13.- Rotary derivatives of the model tested in the Langley free-flight tunnel.



(b)  $\delta_e = -15^\circ$ .

Figure 13.- Concluded.

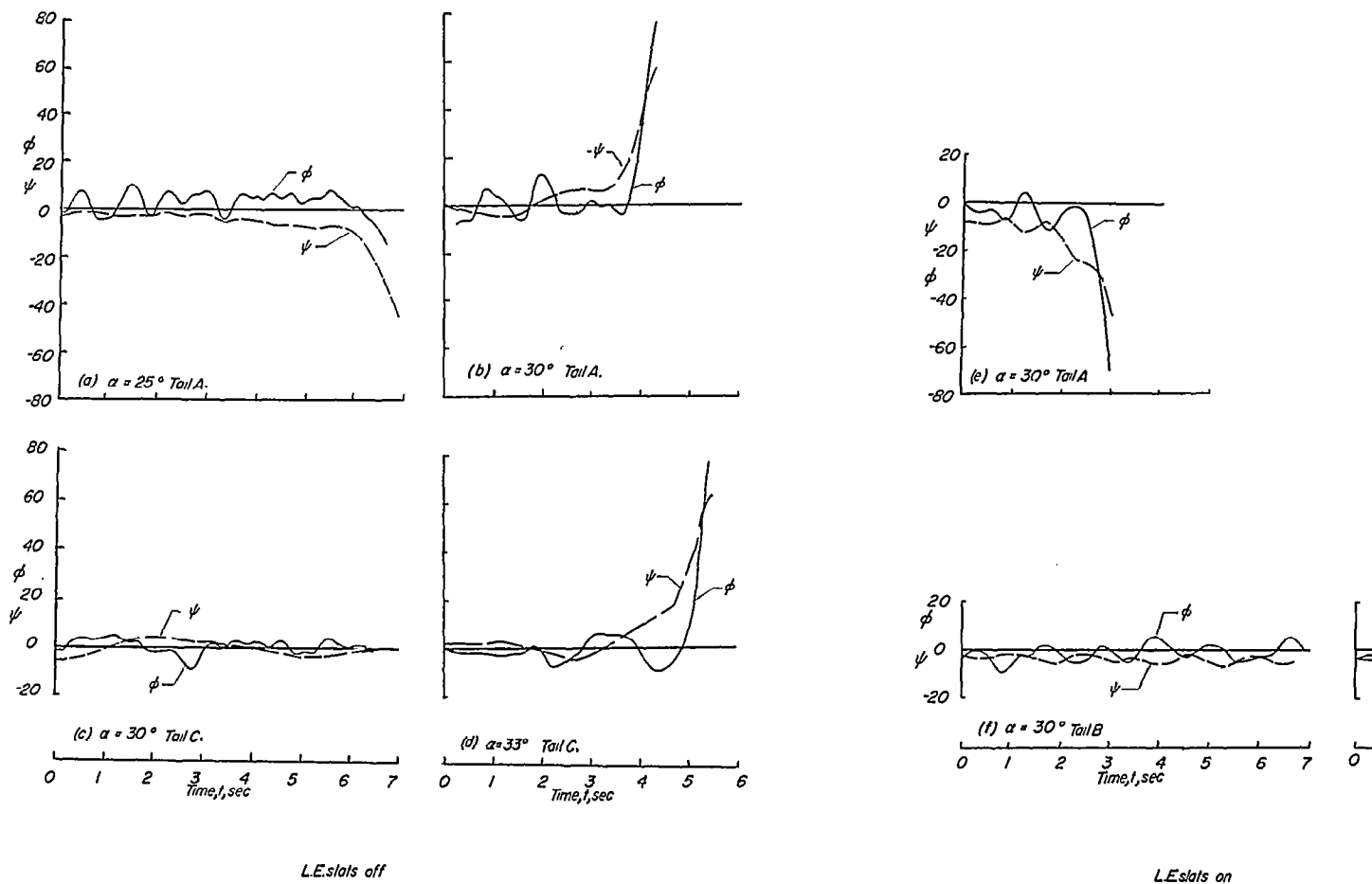


Figure 14.- Flight records of the model tested in the Langley free-flight tunnel.

# SECURITY INFORMATION

~~CONFIDENTIAL~~

3 1176 00159 4085

~~CONFIDENTIAL~~